Inorganic Chemistry

Article

pubs.acs.org/IC

Synthesis, Crystal Chemistry, and Magnetic Properties of $RE_7Li_8Ge_{10}$ and $RE_{11}Li_{12}Ge_{16}$ (RE = La–Nd, Sm): New Members of the $[REGe_2]_n[RELi_2Ge]_m$ Homologous Series

Sheng-Ping Guo,[†] Tae-Soo You,[†,‡] Ya-Ho Jung,[‡] and Svilen Bobev[†,*]

[†]Department of Chemistry and Biochemistry, University of Delaware, Newark, Delaware 19716, United States

[‡]Department of Chemistry, Chungbuk National University, Cheongju, Chungbuk, 361-763, South Korea

Supporting Information

ABSTRACT: Eight new rare-earth metal–lithium–germanides belonging to the $[REGe_2]_n[RELi_2Ge]_m$ homologous series have been synthesized and structurally characterized by single-crystal X-ray diffraction. The structures of the title compounds can be rationalized as linear intergrowths of imaginary $RELi_2Ge$ ($MgAl_2Cu$ structure type) and $REGe_2$ (AlB_2 structure type) slabs. The compounds with general formula $RE_7Li_8Ge_{10}$ (RE = La–Nd, Sm), i.e., $[REGe_2]_3[RELi_2Ge]_4$, crystallize in the orthorhombic space group *Cmmm* (No. 65) with a new structure type. Similarly, the compounds with general formula $RE_{11}Li_{12}Ge_{16}$ (RE = Ce–Nd), i.e., $[REGe_2]_5[RELi_2Ge]_6$, crystallize in the orthorhombic space group *Immm* (No. 71) also with its own structure type. Temperature-dependent DC magnetization measurements indicate Curie–Weiss paramagnetism in the high-temperature regime and hint at complex magnetic ordering at low temperatures. The measured effective moments are consistent with RE^{3+} ground states in all cases. The experimental results have been complemented by tight-binding linear muffin-tin orbital (TB–LMTO) electronic structure calculations.

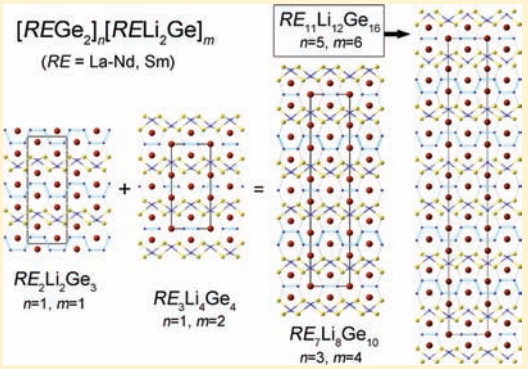

INTRODUCTION

One of the most fascinating traits of the crystal chemistry of many ternary and quaternary intermetallic compounds is that their complex structures can often be recognized as intergrowths (or variants) of simpler structures.[1] In fact, series of compounds can be regarded as homologues, enabling the "design" of a new compound with a predetermined structure/composition and (to some extent) properties. There are many such examples among borides, silicides, germanides, etc., such as $Nd_3Co_{13}B_2$ (i.e., a member of the $RE_{m+1}Co_{5m+3}B_2$ series), whose structure can be characterized by alternate stacking of $NdCo_5$ ($CaCu_5$ type[2]) and $NdCo_3B_2$ ($CeCo_3B_2$ type[2]) slabs.[3] Similarly, $La_3Ru_8B_6$ and $Y_3Os_8B_6$ can be identified as the 2:1 intergrowths of the $CeCo_3B_2$-like and $CeAl_2Ga_2$-like slabs.[4] $RE[AuAl_2]_nAl_2(Au_xSi_{1-x})_2$ and $RE[AuAl_2]_nSi_2(Au_xSi_{1-x})_2$ are readily understood as the combinations of antifluorite-type $AuAl_2$[2] and $BaAl_4$-type[2] slabs and $AuAl_2$ and $CeNiSi_2$ slabs, respectively.[5] Recent work from our laboratory has revealed the existence of the homologous series $[AInGe]_n[A_2InGe_2]_m$ (A = Ca, Sr, Ba, Eu, or Yb),[6] where the structures can be viewed as intergrowths of TiNiSi- and Mo_2FeB_2-like fragments[2] as well as the $[REGe_2]_n[RELi_2Ge]_m$ series (RE = La–Nd, Sm),[7] whose structures can be "cut" into slabs resembling the known AlB_2 and $MgAl_2Cu$ (aka Re_3B[2]) structure types.

In an earlier paper, we reported on 10 compounds belonging to two families, $RE_2Li_2Ge_3$ and $RE_3Li_4Ge_4$ (RE = La–Nd, Sm).[7] They are the simplest members of the above-mentioned homologous series with n = 1 and m = 1 for the $RE_2Li_2Ge_3$ compounds and with n = 1 and m = 2 in the case of $RE_3Li_4Ge_4$. With this paper, we present the synthesis, structural characterization, and magnetic susceptibilities of the higher homologues with n = 3 and m = 4, i.e., the $RE_7Li_8Ge_{10}$ family ($[REGe_2]_3[RELi_2Ge]_4$) and the $RE_{11}Li_{12}Ge_{16}$ family ($[REGe_2]_5[RELi_2Ge]_6$) which occurs for n = 5 and m = 6, respectively. Noteworthy, both crystallize in orthorhombic symmetry with new structure types. The structural relationships between them and other structures are presented. Analysis of the chemical bonding, based on the electronic structure calculation using the tight-binding linear muffin-tin orbital (TB-LMTO) method,[8] is also discussed.

EXPERIMENTAL SECTION

Synthesis. The starting materials were pure metals from Ames Lab, Alfa, or Aldrich (>99.9 wt.%), which were used as received. Li metal was an exception; its surface tarnished even inside an argon-filled glovebox (due to N_2 contamination), and the Li_3N film had to be carefully cleaned with a blade every time when the Li rod was cut into pieces. As a common practice, mixtures of the elements with the desired stoichiometric ratios (total weight ca. 500 mg) were sealed in clean niobium tubes. Welding of the niobium tubes was done using the

Received: March 19, 2012
Published: June 4, 2012

   dx.doi.org/10.1021/ic300566x | *Inorg. Chem.* 2012, 51, 6821–6829

Table 1. Selected Crystal Data and Structure Refinement Parameters for Compounds of the $RE_7Li_8Ge_{10}$ (RE = La–Nd, Sm) Series

empirical formula	$La_7Li_8Ge_{10}$	$Ce_7Li_8Ge_{10}$	$Pr_7Li_8Ge_{10}$	$Nd_7Li_8Ge_{10}$	$Sm_7Li_8Ge_{10}$
fw, g mol^{-1}	1753.79	1762.26	1767.79	1791.10	1833.87
space group	*Cmmm* (No. 65)	*Cmmm* (No. 65)	*Cmmm* (No. 65)	*Cmmm* (No. 65)	*Cmmm* (No. 65)
λ, Å	0.71073	0.71073	0.71073	0.71073	0.71073
T, K	200(2)	200(2)	200(2)	200(2)	200(2)
a, Å	6.975(2)	6.923(5)	6.888(2)	6.8859(14)	6.8148(6)
b, Å	34.029(9)	33.67(2)	33.486(9)	33.450(7)	33.041(3)
c, Å	4.5172(12)	4.466(3)	4.4376(12)	4.4289(9)	4.3693(4)
V, Å^3	1072.2(5)	1041.1(12)	1023.5(5)	1020.1(4)	983.8(2)
Z	2	2	2	2	2
ρ_{calcd}, g cm^{-3}	5.432	5.622	5.736	5.831	6.191
μ (Mo Kα), cm^{-1}	273.5	291.1	307.0	319.0	355.0
GOF on F^2	0.981	1.006	1.045	1.050	0.966
R_1 [$I > 2\sigma(I)$][a]	0.0240	0.0167	0.0233	0.0206	0.0161
wR_2 [$I > 2\sigma(I)$][a]	0.0452	0.0404	0.0494	0.0412	0.0355
R_1 [all data][a]	0.0385	0.0212	0.0295	0.0301	0.0221
wR_2 [all data][a]	0.0500	0.0417	0.0516	0.0437	0.0365

[a] $R_1 = \sum||F_o| - |F_c||/\sum|F_o|$, $wR_2 = [\sum[w(F_o^2 - F_c^2)^2]/\sum[w(F_o^2)^2]]^{1/2}$, and $w = 1/[\sigma^2F_o^2 + (A\cdot P)^2 + B\cdot P]$, $P = (F_o^2 + 2F_c^2)/3$; A and B are weight coefficients. For additional information, see the CIF in the Supporting Information.

TIG process under argon (>99.999%) atmosphere. The welded Nb containers were subsequently enclosed in fused silica tubes, which were flame sealed under vacuum (below discharge). The evacuated tubes with the mixtures inside were heated in programmable tube furnaces to temperatures on the order of 1223–1273 K (ramp rate of 200°/h) and allowed to homogenize for 5 h. Afterward, the temperature was slowly lowered to 1203–1223 K, at which point the furnaces were shut off and allowed to radiatively cool to room temperature.

The above-mentioned heat treatment can produce pure (or nearly pure) phase material of $La_7Li_8Ge_{10}$, $Ce_7Li_8Ge_{10}$, and $Pr_7Li_8Ge_{10}$. $Nd_7Li_8Ge_{10}$ was always attained as a major phase, while $Sm_7Li_8Ge_{10}$ was only obtained as a minor phase. All attempts to synthesize phase-pure $RE_7Li_8Ge_{10}$ (RE = Nd, Sm) failed. In the latter two cases, the reactions always yielded complex mixtures with other ternary compounds, such as RE_4LiGe_4, $RE_2Li_2Ge_3$, or $RE_3Li_4Ge_4$ (RE = Nd, Sm). $Nd_{11}Li_{12}Ge_{16}$, the first known representative of the $RE_{11}Li_{12}Ge_{16}$ family, was also identified as a minor product of such reaction. $Ce_{11}Li_{12}Ge_{16}$ and $Pr_{11}Li_{12}Ge_{16}$ also could not be produced as phase-pure material. Attempts to find a remedy for the synthetic challenges included use of arc-melted "*RE*-Ge" precursors (RE = Nd, Sm); however, the results were similar with the reactions started from the elements. The greatest difficulty that could not be overcome is believed to be the low boiling point of Li relative to the melting point of Ge and the rare-earth metals. Considering that and the very close compositions/similarities in the structures of $RE_2Li_2Ge_3$, $RE_3Li_4Ge_4$, $RE_7Li_8Ge_{10}$, and $RE_{11}Li_{12}Ge_{16}$, it is not surprising that the outcome of each experiment is strongly dependent on extreme precision in each step. This issue has been previously discussed in several earlier papers as well.[7,9–11]

According to the powder X-ray diffraction patterns for specimens kept under an inert atmosphere and after several days of exposure to air, the title compounds are air stable for periods exceeding 1 week.

Crystallographic Studies. X-ray powder diffraction patterns were taken at room temperature on a Rigaku MiniFlex powder diffractometer using Cu Kα radiation (θ–θ scan mode with a step size of 0.05° and a rate of 5 s/step). The instrument was enclosed and operated inside a glovebox, enabling us to handle air-sensitive materials. The collected powder patterns were primarily used for phase identification of the reaction products—these analyses were carried out using the JADE 6.5 software package.

Single-crystal X-ray diffraction data were collected at 200 K using a Bruker SMART CCD-based diffractometer (3-circle goniometer; monochromated Mo Kα_1 radiation (λ = 0.71073 Å)). First, several crystals from each batch were selected and checked before the best ones were chosen for further analysis. Data collection was done with Bruker's SMART software.[12] Data reduction and integration as well as global unit cell refinements were carried out using SAINT.[13] SADABS was used for semiempirical absorption correction based on equivalents.[14] Structures were solved by direct methods and refined to convergence by full matrix least-squares methods on F^2, as implemented in SHELXL.[15] Refined parameters included the scale factor, atomic positions with anisotropic displacement parameters (except for Li), extinction coefficient, and occupancy factors (where needed).

On this note, we draw attention to the fact that the refinements of all $RE_7Li_8Ge_{10}$ structures proceeded smoothly. The equivalent isotropic displacement parameters were nearly identical for all atoms, and final difference Fourier maps were flat with highest maxima and minima not larger than 1–1.5 e^-/Å^3. However, for all three members of the $RE_{11}Li_{12}Ge_{16}$ series, the isotropic displacement parameters of one of the Li atoms, Li3, were abnormally small. When freed, the occupancy factors of the Li sites showed that they exceed full occupancy by 70–80%. A similar problem was reported recently in the structure of the $RE_3Li_4Ge_4$ compounds, where a small Li–Ge positional disorder (i.e., $RE_3Li_{4-x}Ge_{4+x}$) was suggested.[7] In this case too, the supposition of a small admixture of Li and Ge (on the Li site) was verified through refinements that converged to a statistical 95:5 mixture of Li and Ge. Considering that, closer attention was paid to site occupation factors in the structures of the $RE_7Li_8Ge_{10}$ (RE = La–Nd, Sm) compounds. In all five cases though, site occupation factors were checked carefully by freeing the site occupancy of an individual site whereas the remaining parameters were kept fixed. Such refinements indicated no significant deviations from 100%.

In the last refinement cycles, atomic positions were standardized by employing *STRUCTURE TIDY*.[16] Important crystallographic data, atomic positions, selected interatomic distances, and atomic displacement parameters of the series are listed in Tables 1–6. CIFs have also been deposited with Fachinformationszentrum Karlsruhe, 76344 Eggenstein-Leopoldshafen, Germany (fax (49) 7247–808–666; e-mail crysdata@fiz.karlsruhe.de): depository numbers CSD-424320 for $La_7Li_8Ge_{10}$; CSD-424317 for $Ce_7Li_8Ge_{10}$; CSD-424322 for $Pr_7Li_8Ge_{10}$; CSD-424318 for $Nd_7Li_8Ge_{10}$; CSD-424321 for $Sm_7Li_8Ge_{10}$; CSD-424319 for $Ce_{11}Li_{12}Ge_{16}$; CSD-424323 for $Pr_{11}Li_{12}Ge_{16}$; and CSD-424324 for $Nd_{11}Li_{12}Ge_{16}$.

Magnetic Susceptibility Measurements. Field-cooled DC magnetization measurements were performed in a Quantum Design PPMS from 5 to 300 K in an applied magnetic field of 5000 Oe. To ensure reproducibility, specimens from at least two different reaction batches were measured. In all cases, freshly prepared polycrystalline

dx.doi.org/10.1021/ic300566x | *Inorg. Chem.* 2012, 51, 6821–6829

Table 2. Atomic Coordinates and Equivalent Isotropic Displacement Parameters (U_{eq}[b]) for $Ce_7Li_8Ge_{10}$[a]

atom	site	x	y	z	U_{eq}/Å^2
Ce1	4*j*	0	0.1605(1)	1/2	0.009(1)
Ce2	4*j*	0	0.2790(1)	1/2	0.008(1)
Ce3	4*i*	0	0.4421(1)	0	0.009(1)
Ce4	2*a*	0	0	0	0.009(1)
Ge1	8*p*	0.1812(1)	0.2158(1)	0	0.009(1)
Ge2	4*j*	0	0.3731(1)	1/2	0.010(1)
Ge3	4*i*	0	0.0939(1)	0	0.010(1)
Ge4	4*h*	0.3168(1)	0	1/2	0.009(1)
Li1	8*q*	0.1887(10)	0.0749(2)	1/2	0.009(2)
Li2	8*p*	0.3129(10)	0.1434(2)	0	0.013(2)

[a]Data for the remaining four compounds of the series, $RE_7Li_8Ge_{10}$ (*RE* = La, Pr, Nd, Sm), is provided in the Supporting Information. [b]U_{ij} is defined as one-third of the trace of the orthogonalized U_{ij} tensor

Table 3. Important Interatomic Distances for $Ce_7Li_8Ge_{10}$[a]

atom pair	distance (Å)	atom pair	distance (Å)
Ge1−Ge1	2.490(2)	Ce1−Ge3	3.165(1) × 2
Ge1−Ge1	2.509(2)	Ce1−Ge1	3.167(1) × 4
Ge4−Ge4	2.537(2)	Ce1−Li2	3.164(5) × 4
Li1−Ge2	2.777(8)	Ce1−Li1	3.164(8) × 2
Li1−Ge3	2.665(4) × 2	Ce2−Ge1	3.145(1) × 4
Li1−Ge4	2.674(7)	Ce2−Ge2	3.169(2)
Li2−Ge1	2.603(8)	Ce2−Ge1	3.329(1) × 4
Li2−Ge2	2.641(4) × 2	Ce3−Ge2	3.223(1) × 2
Li2−Ge3	2.734(7)	Ce3−Ge4	3.225(1) × 4
		Ce3−Li1	3.156(5) × 4
		Ce3−Li2	3.158(8) × 2
		Ce4−Ge4	3.130(2) × 4
		Ce4−Ge3	3.162(2) × 2

[a]Data for the remaining four compounds of the series, $RE_7Li_8Ge_{10}$ (*RE* = La, Pr, Nd, Sm), is provided in the Supporting Information.

Table 4. Selected Crystal Data and Structure Refinement Parameters for $RE_{11}Li_{12}Ge_{16}$ (*RE* = Ce, Pr, Nd) Series[a]

empirical formula	$Ce_{11}Li_{12}Ge_{16}$[c]	$Pr_{11}Li_{12}Ge_{16}$[c]	$Nd_{11}Li_{12}Ge_{16}$[c]
fw/g mol^{-1}	2786.04	2794.73	2831.36
space group	*Immm* (No. 71)	*Immm* (No. 71)	*Immm* (No. 71)
λ/Å	0.71073	0.71073	0.71073
T/K	200(2)	200(2)	200(2)
a/ Å	4.4681(4)	4.4389(17)	4.4139(8)
b/ Å	6.9249(6)	6.899(3)	6.8688(13)
c/ Å	52.492(5)	52.23(2)	51.973(10)
V/ Å^3	1624.2(2)	1599.7(11)	1575.7(5)
Z	2	2	2
ρ_{calcd}/ g cm^{-3}	5.697	5.802	5.967
μ (Mo Kα)/ cm^{-1}	295.8	311.3	327.2
GOF on F^2	1.130	1.100	1.067
R_1 [$I > 2\sigma(I)$][b]	0.0245	0.0245	0.0285
wR_2 [$I > 2\sigma(I)$][b]	0.0548	0.0477	0.0542
R_1 [all data][b]	0.0361	0.0376	0.0510
wR_2 [all data][b]	0.0750	0.0598	0.0669

[a]For simplicity, the $RE_{11}Li_{12}Ge_{16}$ formula is used throughout the text, but this table refers to the refinements of $RE_{11}Li_{12-x}Ge_{16+x}$ ($x \approx 0.2$). [b]$R_1 = \sum||F_o| - |F_c||/\sum|F_o|$; $wR_2 = [\sum[w(F_o^2 - F_c^2)^2]/\sum[w(F_o^2)^2]]^{1/2}$, and $w = 1/[\sigma^2F_o^2 + (A\cdot P)^2 + B\cdot P]$, $P = (F_o^2 + 2F_c^2)/3$; *A* and *B* are weight coefficients. For additional information, see the CIF in the Supporting Information. [c]Refined formulas: $Ce_{11}Li_{11.81}Ge_{16.19(2)}$, $Pr_{11}Li_{11.82}Ge_{16.18(2)}$, and $Nd_{11}Li_{11.82}Ge_{16.18(2)}$.

Table 5. Atomic Coordinates and Equivalent Isotropic Displacement Parameters (U_{eq}[b]) for $Ce_{11}Li_{12}Ge_{16}$[a]

atom	site	x	y	z	U_{eq}/ Å^2
Ce1	4*j*	1/2	0	0.10282(1)	0.008(1)
Ce2	4*j*	1/2	0	0.17872(1)	0.008(1)
Ce3	4*j*	1/2	0	0.46291(1)	0.008(1)
Ce4	4*i*	0	0	0.28262(1)	0.008(1)
Ce5	4*i*	0	0	0.35843(1)	0.007(1)
Ce6	2*a*	0	0	0	0.008(1)
Ge1	8*l*	0	0.1813(1)	0.13832(2)	0.008(1)
Ge2	8*l*	0	0.3188(1)	0.18211(2)	0.008(1)
Ge3	4*j*	1/2	0	0.23916(3)	0.009(1)
Ge4	4*i*	0	0	0.06021(3)	0.010(1)
Ge5	4*i*	0	0	0.41863(3)	0.010(1)
Ge6	4*h*	0	0.1833(2)	1/2	0.009(1)
Li1	8*l*	0	0.187(2)	0.2285(3)	0.014(3)
Li2	8*l*	0	0.313(2)	0.0915(3)	0.008(3)
Li3[c]	8*l*	0	0.310(2)	0.4526(3)	0.035(5)

[a]Data for the remaining two compounds of the series, $RE_{11}Li_{12}Ge_{16}$ (*RE* = Pr, Nd), is provided in the Supporting Information. [b]U_{ij} is defined as one-third of the trace of the orthogonalized U^{ij} tensor. [c]Refined as a statistical mixture of Li:Ge = 0.952(6):0.048.

Table 6. Important Interatomic Distances for $Ce_{11}Li_{12}Ge_{16}$[a]

atom pair	distance (Å)	atom pair	distance (Å)
Ge1−Ge2	2.488(1)	Ce1−Ge4	3.161(1) × 2
Ge1−Ge1	2.511(2)	Ce1−Ge1	3.1686(8) × 4
Ge2−Ge2	2.509(2)	Ce1−Li2	3.17(1) × 4
Ge6−Ge6	2.539(2)	Ce1−Li3	3.19(1) × 2
		Ce2−Ge2	3.1460(7) × 4
Li1−Ge2	2.60(2)	Ce2−Ge3	3.172(2)
Li1−Ge3	2.644(9) × 2	Ce2−Ge1	3.3263(9) × 4
Li1−Ge3	2.75(2)	Ce3−Ge5	3.224(1) × 2
Li2−Ge1	2.59(2)	Ce3−Ge6	3.225(1) × 4
Li2−Ge5	2.635(8) × 2	Ce3−Li3	3.15(1) × 4
Li2−Ge4	2.72(2)	Ce3−Li2	3.14(2) × 2
Li3−Ge6	2.64(2)	Ce4−Ge2	3.1609(8) × 4
Li3−Ge4	2.677(9) × 2	Ce4−Ge3	3.193(1) × 2
Li3−Ge5	2.79(2)	Ce4−Li1	3.13(2) × 2
		Ce4−Li1	3.17(2) × 4
		Ce5−Ge1	3.1450(7) × 4
		Ce5−Ge5	3.160(2)
		Ce5−Ge2	3.3307(8) × 4
		Ce6−Ge6	3.130(1) × 4
		Ce6−Ge4	3.161(1) × 2

[a]Data for the remaining two compounds of the series, $RE_{11}Li_{12}Ge_{16}$ (*RE* = Pr, Nd), is provided in the Supporting Information.

materials (phase purity verified via powder X-ray diffraction) were secured in gel capsules. Raw magnetization data were collected for the holder contribution and converted to molar susceptibility (χ_m = M/H; units of emu/mol). For $Ce_7Li_8Ge_{10}$, zero-field-cooled measurements were carried out from 5 to 35 K under the same applied field. Field sweep for the same specimen was done at 2 K up to applied magnetic fields of 70 kOe.

Computational Details. Tight-binding linear muffin-tin orbital (TB-LMTO) calculations were carried out using the LMTO47 program.[17] This package employs the atomic sphere approximation (ASA) method in which space is filled with overlapping Wigner−Seitz (WS) atomic spheres.[18] The symmetry of the potential is considered spherical inside each WS sphere, and a combined correction is used to take into account the overlapping part. The radii of WS spheres were obtained by requiring that the overlapping potential be the best

dx.doi.org/10.1021/ic300566x | Inorg. Chem. 2012, 51, 6821−6829

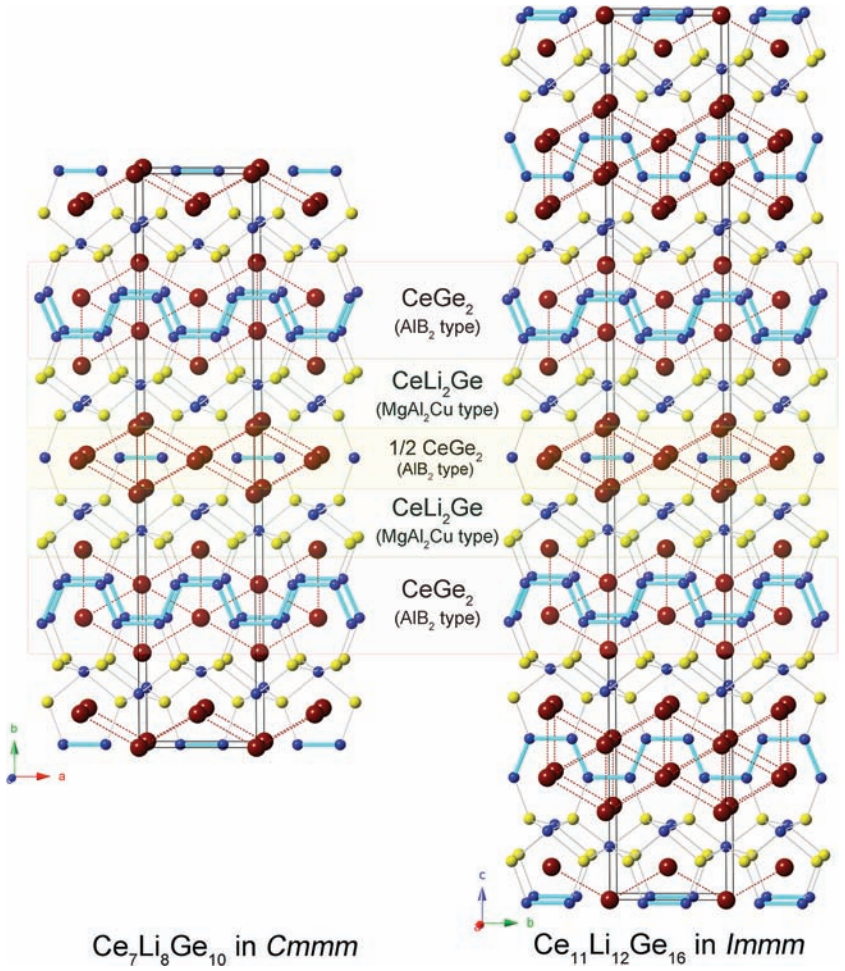

Figure 1. Ball-and-stick representations of the orthorhombic structures of the $RE_7Li_8Ge_{10}$ and $RE_{11}Li_{12}Ge_{16}$ (*RE* = La–Nd, Sm) compounds. Unit cells are outlined. *RE* atoms are shown as maroon spheres, and Ge atoms are drawn as blue spheres. Li atoms are shown in yellow. Stacking sequence of slabs with compositions $REGe_2$ (AlB_2 structure type) and $RELi_2Ge$ ($MgAl_2Cu$ structure type) compounds are highlighted; they allow for rationalizing the structures as members of the $[REGe_2]_n[RELi_2Ge]_m$ homologous series.

possible approximation to the full potential and were determined by an automatic procedure. Exchange and correlation were treated by the local density approximation (LDA).[19] All relativistic effects, except spin–orbit coupling, were taken into account using a scalar relativistic approximation.[20] WS radii are as follows: La = 2.06–2.14 Å, Li = 1.44–1.48 Å, Ge = 1.48–1.72 Å for $La_7Li_8Ge_{10}$ and Ce = 2.03–2.11 Å, Li = 1.41–1.47 Å, Ge = 1.48–1.73 Å for $Ce_{11}Li_{12}Ge_{16}$. The *k*-space integrations were conducted by the tetrahedron method,[21] and the self-consistent charge density was obtained using 12 × 12 × 12 *k* points for $La_7Li_8Ge_{10}$ and 8 × 12 × 12 *k* points for $Ce_{11}Li_{12}Ge_{16}$ in the Brillouin zone. The La 6p, Ce 6p, Ge 4d, and Li 2p orbitals were treated by the Löwdin downfolding technique, and the Ce 4f states were treated as core orbitals.

RESULTS AND DISCUSSION

Structures. Crystallographic data for the $RE_7Li_8Ge_{10}$ (*RE* = La–Nd, Sm) compounds are summarized in Tables 1–3. Their structure is with the orthorhombic space group *Cmmm* (own structure type, Pearson code *oC*50). $RE_{11}Li_{12}Ge_{16}$ (*RE* = Ce–Nd) also crystallize with their own structure type (space group *Immm*, Pearson code *oI*78), and relevant crystallographic information for the three refined structures is given in Tables 4–6. Figure 1 shows structural representations and emphasizes how closely related both structures are; despite the different extended symmetry, both structures can be "cut" into identical slabs resembling the known AlB_2 and $MgAl_2Cu$ (aka Re_3B) structure types.[2] This analogy will be discussed further, after the important characteristics of the two bonding arrangements are elaborated. For convenience here, our discussion will focus on $Ce_7Li_8Ge_{10}$ and $Ce_{11}Li_{11}Ge_{16}$, which will allow for the unambiguous side-by-side comparison.

The asymmetric unit of the $Ce_7Li_8Ge_{10}$ structure contains 10 crystallographically unique sites: four for the rare-earth metal atoms, two for the lithium atoms, and the remaining four for the germanium atoms. The four Ce atoms exhibit three types of coordination environments: Ce1 and Ce3 atoms are coordinated by six neighboring Ge atoms in trigonal prismatic fashion, the Ce4 atoms are octahedrally coordinated, whereas the Ce2 atoms are with nine neighboring Ge atoms, arranged as distorted monocapped square prisms, respectively. If Li atoms are also included in the coordination sphere, the Ce1, Ce2, Ce3, and Ce4 atoms have coordination numbers of 12, 9, 12, and 6, respectively (Table 3). Both Li atoms are tetrahedrally surrounded by four Ge atoms; Li2 atoms have no contact with Ge1 and Ge4. There are three types of Li1–Ge and Li2–Ge distances. The Li–Ge distances fall in the range of 2.543(8)–2.831(13) Å, with the Li1–Ge2 and Li2–Ge3 contacts being the longest among Li1–Ge and Li2–Ge, respectively. Considering the Pauling's covalent radii of Li (1.225 Å) and Ge (1.242 Å),[22] the interactions between Li and Ge atoms have

dx.doi.org/10.1021/ic300566x | *Inorg. Chem.* 2012, 51, 6821–6829

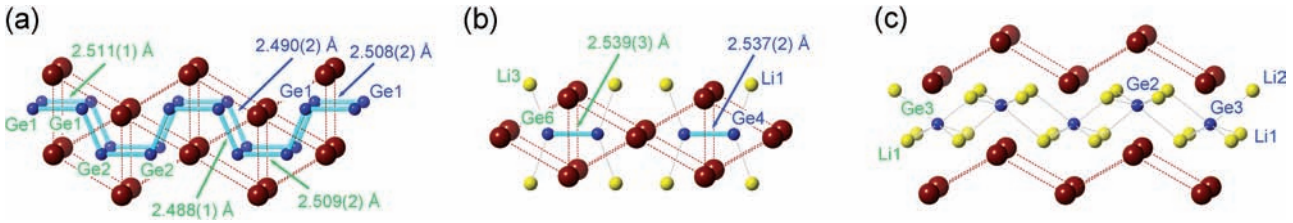

Figure 2. Three distinct (poly)anionic fragments in the structures of the $RE_7Li_8Ge_{10}$ and $RE_{11}Li_{12}Ge_{16}$ (*RE* = La–Nd, Sm) compounds. $^1_\infty[Ge_2]$ chains (a) and $[Ge_2]$ dumbbells (b) are emphasized. Corresponding labels and interatomic distances within the two units are shown as follows: blue for $Ce_7Li_8Ge_{10}$ and green for $Ce_{11}Li_{12}Ge_{16}$. Within the $RELi_2Ge$ slab (c), the Li atoms (in yellow) are shown as connected to four neighboring Ge atoms, forming slabs of fused $LiGe_4$ tetrahedra.

significant covalent character; this argument is also verified by the results of the electronic structure calculations (vide infra).

The four crystallographically unique Ge atoms form three distinct anionic motifs, which are represented in Figure 2. Ge1 atoms form infinite $^1_\infty[Ge_2]$ chains of alternating *trans* and *cis* bonds; the Ge4 atoms form Ge_2 dimers, both aligned in a direction parallel to the *a* axis. Ge1 and Ge4 are at the centers of trigonal prisms formed by the rare-earth metal atoms, as expected for slabs with AlB_2-like topology. The Ge2 and Ge3 atoms are isolated (i.e., not connected to other Ge atoms) and have similar coordination environments; both are surrounded by six Li atoms, three close, and two distant Ce atoms can also be included in the coordination sphere. This arrangement is reminiscent with the $MgAl_2Cu$ (aka Re_3B) structure type.[2]

The *cis*- and *trans*-Ge1–Ge1 bonds within the $^1_\infty[Ge_2]$ chains in $Ce_7Li_8Ge_{10}$ are 2.508(2) and 2.490(2) Å long, respectively. Notice that the *cis* bond is a bit longer than the *trans* bond (Figure 2). These distances are close to the 2.4695(16)–2.500(3) (*trans*) and 2.5058–2.524(3) Å (*cis*) Ge–Ge distances reported for the structures of the closely related $RE_2Li_2Ge_3$.[7] Similarly, these distances are comparable with the Ge–Ge distances in $RELiGe_2$ (d_{Ge-Ge} = 2.4948(5)–2.5318(8) Å),[9] $SrLi_{0.95}In_{0.05}Ge_2$ (d_{Ge-Ge} = 2.485(2)–2.508(2) Å), and $Sr_2Li_{1.45}In_{0.55}Ge_3$ (d_{Ge-Ge} = 2.498(2)–2.514(2) Å),[11] where *cis*–*trans* or zigzag chains are present. The Ge_2 dimers in $Ce_7Li_8Ge_{10}$ are slightly longer than the Ge–Ge bonds in the $^1_\infty[Ge_2]$ chains at 2.537(2) Å; this value matches very well the Ge–Ge contacts in other rare-earth metal germanides containing Ge_2 dimers, such as $RE_3Li_4Ge_4$ (d_{Ge-Ge} = 2.514(2)–2.524(2) Å),[7] and RE_2MgGe_2 (d_{Ge-Ge} = 2.506(2)–2.548(1) Å).[23] The Ge–Ge distances show very little dependence on the decreasing unit cell volume (lanthanide contraction) on going from La to Sm (Tables 1 and 3).

The asymmetric unit of the $Ce_{11}Li_{12}Ge_{16}$ structure contains 15 crystallographically unique sites, occupied by six rare-earth metal atoms, six germanium atoms, and three lithium atoms. Due to the larger number of atoms in the unit cell and the differences in the site symmetry/multiplicity, direct comparison with $Ce_7Li_8Ge_{10}$ is somewhat hindered. However, the structural representation in Figure 1 clearly shows that the two structures are "stacking" variants of the same building blocks—$CeGe_2$ (AlB_2-like) and $CeLi_2Ge$ ($MgAl_2Cu$-like) fragments, which in $Ce_{11}Li_{12}Ge_{16}$ are arranged along the *c* direction. The coordination environments of the rare-earth metal atoms are identical to the ones already described—Ce1, Ce3, and Ce4 have six neighboring Ge atoms forming distorted trigonal prisms (just like Ce1 and Ce3 in $Ce_7Li_8Ge_{10}$), Ce6 atoms are found in octahedra of the nearest Ge atoms (just like Ce4 in $Ce_7Li_8Ge_{10}$), and Ce2 and Ce5 are 9-coordinated. The three independent Li atoms are again tetrahedrally surrounded by Ge atoms, with the only difference being that the Li1 has contacts only with Ge1, Ge2, and Ge3, Li2 neighbors only Ge1 and Ge5, while the Li3 atoms have contacts with Ge4 and Ge6, respectively (Table 3).

The six crystallographically unique Ge atoms again form infinite $^1_\infty[Ge_2]$ chains (Ge1 and Ge2), Ge_2 dimers (Ge6), and Ge3, Ge4, and Ge5 atoms are isolated (Figure 2). Every detail of the $Ce_{11}Li_{12}Ge_{16}$ structure is identical to that of $Ce_7Li_8Ge_{10}$, including the difference in the lengths of the *cis* vs *trans* bonds ($d_{Ge1-Ge1}$ = 2.511(1) Å; $d_{Ge2-Ge2}$ = 2.509(2) Å vs $d_{Ge1-Ge2}$ = 2.488(1) Å). The lengths of the Ge–Ge bonds (within the dimers) also match within the e.s.d. These observations are somewhat puzzling since in the $Ce_{11}Li_{12}Ge_{16}$ structure, as discussed earlier, we found crystallographic evidence for a small admixture of Ge at the Li site. Similar to the compounds of the $RE_3Li_4Ge_4$ series (rather $RE_3Li_{4-x}Ge_{4+x}$),[7] the disorder is very small (Li:Ge ≈ 95:5), and it is practically impossible to discern any geometric differences. However, the slightly higher valence electron concentration (VEC) as a result of this disorder could be expected to augment the bonding characteristics, which is not observed.

Structural Relationships. The structures of the $RE_7Li_8Ge_{10}$ and $RE_{11}Li_{12}Ge_{16}$ compounds can be "tailored" from imaginary slabs with compositions $REGe_2$ (AlB_2-like) and $RELi_2Ge$ ($MgAl_2Cu$-like), as shown in Figure 1. This is not a rigorous application of the intergrowth concept,[1] since the slabs containing Ge_2 dimers must be treated as one-half of the "real" $REGe_2$ motif. Following this interpretation, $RE_2Li_2Ge_3$, $RE_3Li_4Ge_4$, $RE_7Li_8Ge_{10}$, and $RE_{11}Li_{12}Ge_{16}$ can be regarded as members of the homologous series $[REGe_2]_n[RELi_2Ge]_m$, where the already reported $RE_2Li_2Ge_3$ and $RE_3Li_4Ge_4$ are realized for n = 1 and m = 1 and for n = 1 and m = 2, respectively.[7] Herein, the structures of the $RE_7Li_8Ge_{10}$ and $RE_{11}Li_{12}Ge_{16}$ compounds can be identified as $[REGe_2]_n[RELi_2Ge]_m$ with n = 3 and m = 4 and with n = 5 and m = 6. One can notice that $RE_2Li_2Ge_3$ is the simplest member with n = 1 and m = 1, and the three higher homologues are with n:m ratios of 1:2 ($RE_3Li_4Ge_4$), 3:4 ($RE_7Li_8Ge_{10}$), and 5:6 ($Ce_{11}Li_{12}Ge_{16}$), i.e., they are all realized when $m = n + 1$. Therefore, the $[REGe_2]_n[RELi_2Ge]_m$ homologous series can also be represented as $[RE_4Li_4Ge_6]_x[RE_3Li_4Ge_4]_y$ if one considers the structures of $RE_2Li_2Ge_3$ (rewritten as $RE_4Li_4Ge_6$) and $RE_3Li_4Ge_4$ as the basic units. Following this, the $RE_7Li_8Ge_{10}$ and $RE_{11}Li_{12}Ge_{16}$ structures can also be described as linear intergrowths of $RE_4Li_4Ge_6$ and $RE_3Li_4Ge_4$ with ratios of 1:1 and 2:1, respectively. A schematic representation of this idea is shown in Figure S1 (Supporting Information).

On the basis of the above discussions, most likely, the next homologue will be $[REGe_2]_7[RELi_2Ge]_8$ or $[RE_4Li_4Ge_6]_3[RE_3Li_4Ge_4]$, i.e., $RE_{15}Li_{16}Ge_{22}$. Whether this

dx.doi.org/10.1021/ic300566x | *Inorg. Chem.* 2012, 51, 6821–6829

supposition is true or not requires more experimental work and it could very well be that such complex structures can be very difficult to obtain in single-crystalline form.

Electron Count. A good starting point to rationalize the electronic structures of the $RE_7Li_8Ge_{10}$ and $RE_{11}Li_{12}Ge_{16}$ compounds is to employ the Zintl–Klemm concept[24] in a manner similar to what we have done before for $RE_2Li_2Ge_3$ and $RE_3Li_4Ge_4$.[7] This description, of course, does not take into account the fact that *RE* and Li atoms cannot be "ionized" completely and cannot provide all their valence electrons for germanium bonding. Since the same three kinds of Ge anions exist in all structures, the Zintl–Klemm type of "electron bookkeeping" practices should be equally applicable, i.e., the isolated Ge atoms will be assigned as Ge^{4-}, the dimerized Ge atoms as Ge^{3-}, and the ones forming the *cis–trans* chains as Ge^{2-}. Hence, assuming that the rare-earth metals and the lithium are cations, the formula of $RE_7Li_8Ge_{10}$ can be written as $(RE^{3+})_7(Li^+)_8(Ge^{4-})_4(Ge^{3-})_2(Ge^{2-})_4(h^+)$, where h^+ stands for an electron hole. In a similar manner, the formula of $RE_{11}Li_{12}Ge_{16}$ can be written as $(RE^{3+})_{11}(Li^+)_{12}(Ge^{4-})_6(Ge^{3-})_2(Ge^{2-})_8(h^+)$, indicating a shortage of one valence electron as well. Considering that both structures contain $RE_4Li_4Ge_6$ (electron-precise) and $RE_3Li_4Ge_4$ (one electron-deficient) fragments, this apparent electron deficiency is not difficult to understand. The imprecise electron count could also be related to the bonding in the $^1_\infty[Ge_2]$ chains, which somewhat resemble conjugated systems (vide supra). The relatively short Ge–Ge interactions (together with the pattern between the cis and the trans bonds, Figure 2) supports this conclusion. However, all metrics of the structures are virtually identical, despite the electron count in $RE_{11}Li_{12}Ge_{16}$ being slightly altered due to the small admixture of Ge at the Li3 site, making $RE_{11}Li_{12-x}Ge_{16+x}$ ($x \approx 0.2$) approximately 0.6 e^-/formula unit richer, just like $RE_3Li_{4-x}Ge_{4+x}$,[7] and thereby closer to the ideal Zintl limit. Therefore, to better understand these nuances of the chemical bonding of $RE_7Li_8Ge_{10}$ and $RE_{11}Li_{12}Ge_{16}$ (*RE* = La–Nd, Sm), computations based on density functional theory (DFT) were carried, and the results are discussed next.

Bonding and Electronic Structures. The electronic structures of $La_7Li_8Ge_{10}$ and $Ce_{11}Li_{12}Ge_{16}$ were calculated using the TB-LMTO method.[8] The calculated total and partial density of state (DOS) curves together with the crystal orbital Hamilton populations (COHP) for the Ge–Ge and Li–Ge bonds are plotted in Figures 3 and 4, respectively.

As one can expect from the earlier structural discussion, the overall characteristics of the electronic structure of $La_7Li_8Ge_{10}$ very much resembles the features of the lower homologues $La_2Li_2Ge_3$ and $La_3Li_4Ge_4$.[7] First, the Fermi level corresponding to 69 valence electrons is situated at the local DOS minimum (Figure 3a), where the total DOS value can be regarded as an intermediate between the relatively lower DOS value of $La_2Li_2Ge_3$ and the higher DOS value of $La_3Li_4Ge_4$. In the plot, the low-energy region between −11 and −6 eV is predominantly contributed by Ge 4s orbitals, while the region from −4.5 eV and E_F displays significant covalent-type bonding interactions between the anionic components. In addition, some participation of La valence orbitals into orbital mixing below E_F is clearly observed around this region, implying that the La atoms take more than a simple role as electron donors. Such type of cation orbital mixing into the valence band is caused by incomplete electron transfer to anionic elements and is one of the typical features of polar intermetallic

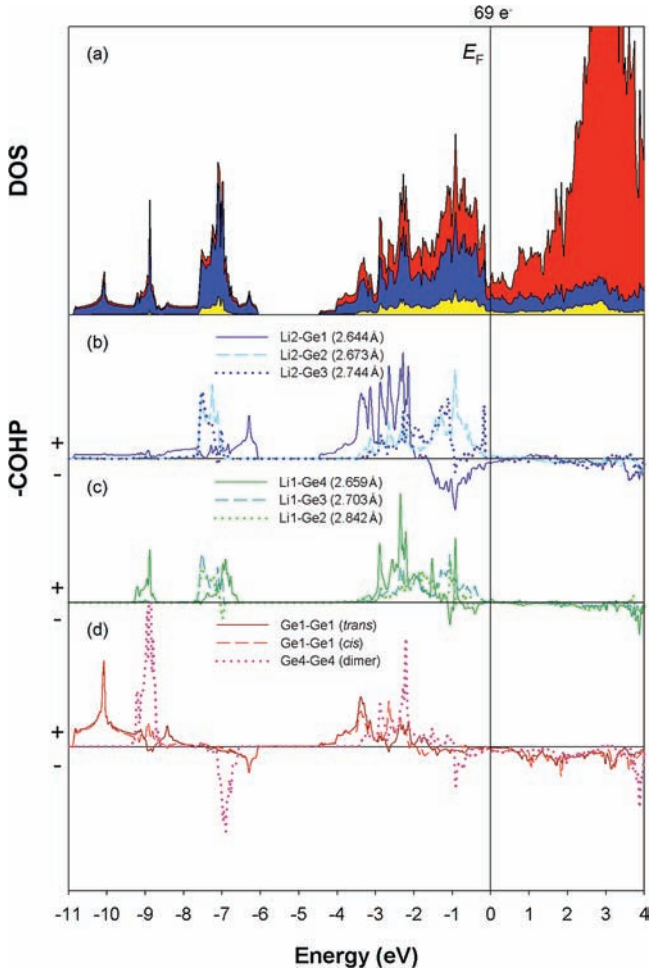

Figure 3. Calculated DOS and COHP for $La_7Li_8Ge_{10}$. Total DOS and partial DOS (La PDOS, red area; Ge PDOS, blue area; Li PDOS, yellow area) are plotted. Fermi level is chosen as the energy reference at 0 eV, and the corresponding number of valence electrons is shown.

compounds.[25] Similar "effect" was previously discussed for $La_2Li_3Ge_3$ and $La_3Li_4Ge_4$[7] and is also evident for $Ce_{11}Li_{12}Ge_{16}$.

COHP curves illustrated in Figure 3b–d represent the bonding within the two similar but slightly different tetrahedra centered by Li1 and Li2, respectively (Figure 3b and 3c), and the two distinct Ge fragments, the $^1_\infty[Ge_2]$ chain, and the Ge_2 dimer. Interestingly, the COHP curves for the Li2–Ge bonding and the Ge–Ge bonding within the chains are nearly identical to those in $La_2Li_2Ge_3$.[7] Here, Li2 is connected to three isolated Ge atoms and one Ge1 atom from the *cis/trans* chain. Notice that COHP of Li2–Ge1 has a weak antibonding character, while the COHP curves for the relatively longer Li2–Ge2 (2.673 Å) and Li2–Ge3 (2.744 Å) are well optimized at E_F. Two Ge1–Ge1 COHP curves representing interactions in the *cis/trans* Ge chain indicate that the antibonding states originated from the *trans* bonds are less populated compared to the *cis* bonds, explaining the slightly longer (weaker) cis-type Ge–Ge interactions. Figure 3c shows COHPs of the other tetrahedron centered by Li1 (bonded to one Ge4 atom-forming dimers and three isolated Ge atoms). The bonding between Li1 and Ge4 displays a weak antibonding character, and other Li1–Ge interactions are nearly optimized. The COHP curve of the Ge4–Ge4 dimer resembles that of the Ge1–Ge1 dimer reported previously in $La_3Li_4Ge_4$.[7]

dx.doi.org/10.1021/ic300566x | *Inorg. Chem.* 2012, 51, 6821–6829

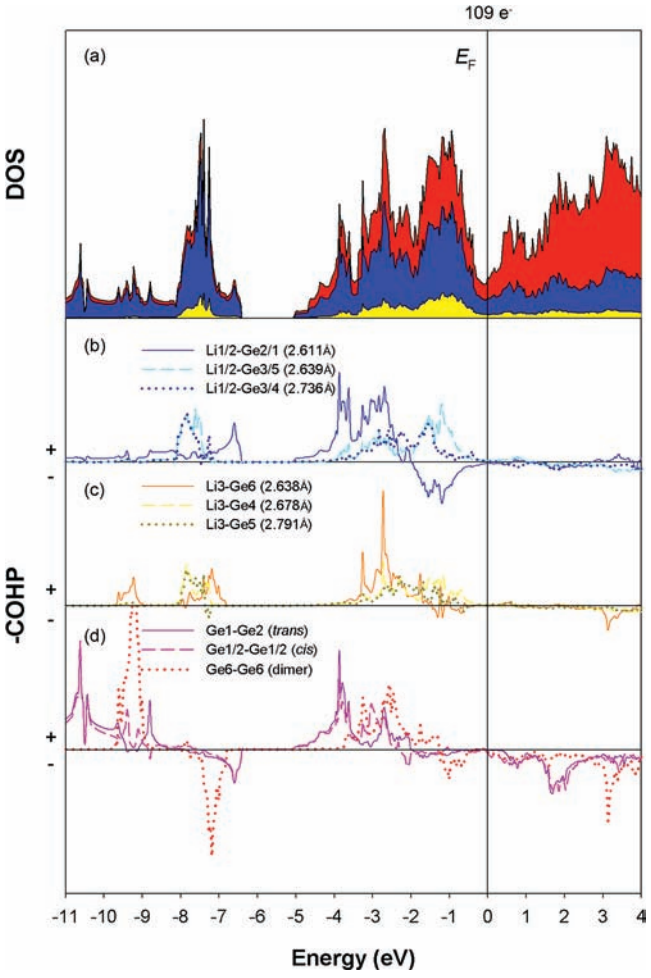

Figure 4. Calculated DOS and COHP for $Ce_{11}Li_{12}Ge_{16}$. Total DOS and partial DOS (Ce PDOS, red area; Ge PDOS, blue area; Li PDOS, yellow area) are plotted. Fermi level is chosen as the energy reference at 0 eV, and the corresponding number of valence electrons is shown.

On the basis of the above analysis, the apparent shortage of a valence electron in $La_7Li_8Ge_{10}$ (recall the electron count $(La^{3+})_7(Li^+)_8(Ge^{4-})_4(Ge^{3-})_2(Ge^{2-})_4(h^+)$ from the Zintl arguments) can be explained; it is obviously stemming from the $La_3Li_4Ge_4$ partial structure, whose influence in the overall (joint) structure is counterbalanced by two $La_2Li_2Ge_3$ slabs ($La_7Li_8Ge_{10}$ = $[La_4Li_4Ge_6][La_3Li_4Ge_4]$), resulting in an improved electronic stability. Previously, we argued that the stoichiometric $RE_3Li_4Ge_4$ was electronically unfavorable,[7] and Li/Ge mixing was necessary to alleviate the shortage of a valence electron. However, the overall electronic structure of $La_7Li_8Ge_{10}$ does not show the signs of an apparent electron deficiency, which could be understood by comparing the valence electron concentrations (VEC): 69 available valence electrons per formula unit of $La_7Li_8Ge_{10}$ (VEC = 2.76 e^-/atom) with an ideal VEC of 2.8 e^-/atom, whereas the 29 valence electrons per formula unit of $La_3Li_4Ge_4$ account for a lower VEC = 2.64 e^-/atom. This implies that the "missing electron" has a more significant impact on the latter structure, while the $La_7Li_8Ge_{10}$ structure successfully adapts to a less-than-optimal number of valence electrons.

Figure 4 displays the total and partial DOS of $Ce_{11}Li_{12}Ge_{16}$, together with COHP curves for various interactions. Overall, the DOS features are similar to that of $La_7Li_8Ge_{10}$, where a significant Ge 4s orbital contribution is shown between −11 and −6 eV and a strong orbital mixing, indicating covalency of the anionic interactions is observed between −5 eV and E_F. Like in $La_7Li_8Ge_{10}$, there are a total of 109 valence electrons per formula unit, while the ideal electron count in $Ce_{11}Li_{12}Ge_{16}$, according the Zintl−Klemm formalism, will be 110. Reformulating this statement in terms of VEC one can see that the ideal VEC (2.82 e^-/atom) and the actual VEC (2.79 e^-/atom) values are very close and can reason that the electronic stability of $Ce_{11}Li_{12}Ge_{16}$ will not be diminished as a result of this presumed "shortage". The local DOS minimum, as depicted in Figure 4a, confirms this line of thinking. Therefore, it is puzzling that this electronic argument is consistent with our crystal structure refinements for $RE_7Li_8Ge_{10}$ (*RE* = La−Nd, Sm), where no Li and Ge mixing can be discerned in any of the 5 refined structures, but such disorder, albeit very small (Li:Ge = 95:5), is seen in all 3 $RE_{11}Li_{12}Ge_{16}$ (*RE* = La−Nd, Sm) refined structures,

Figure 4b and 4c shows the COHP curves representing the different tetrahedra centered by Li1(Li2) and Li3. Li1 is bonded to one Ge2 (Ge1) on the *cis*/*trans* chain and three isolated Ge atoms; Li2 is bonded to Ge1 from the chain and three isolated Ge atoms. Their local coordination environment is virtually identical to that of Li2 in $La_7Li_8Ge_{10}$ (as well as the Li atoms in $La_2Li_2Ge_3$). On the other hand, the coordination around Li3 is identical to that of Li1 in $La_7Li_8Ge_{10}$ (as well as the Li atoms in $La_3Li_4Ge_4$). Not surprisingly, the COHP curves of the Li−Ge bonding in $Ce_{11}Li_{12}Ge_{16}$ and the lower homologues are very much alike. The same is true for the COHP curves representing the infinite $^1_\infty[Ge_2]$ chains and the Ge_2 dimer, as illustrated in Figure 4d. There is no evidence in either the DOS or the COHP curves of $Ce_{11}Li_{12}Ge_{16}$ to corroborate the Ge substitution for Li, suggested from the crystal structure refinements. At present, this remains a poorly understood issue, which calls for more structural/computational work.

Magnetic Susceptibilities. The temperature-dependent DC magnetization measurements were performed on samples of $RE_7Li_8Ge_{10}$ (*RE* = Ce, Pr) within the range from 2 to 300 K under an applied field of 5000 Oe; $La_7Li_8Ge_{10}$ was measured only below 20 K under an applied field of 50 Oe. Reliable data for the remaining phases could not be obtained, since they were not phase pure.

$La_7Li_8Ge_{10}$ is Pauli-like paramagnetic, as expected for a compound with no localized unpaired electrons. The data show no hints at superconductivity down to 1.7 K, and it is not discussed further. In the high-temperature regime, the $\chi(T)$ behavior of the $RE_7Li_8Ge_{10}$ (*RE* = Ce, Pr) follows the Curie−Weiss law $\chi(T) = C/(T - \theta_p)$,[26] as expected for compounds with core 4f electrons. Curie constants (C) and effective magnetic moments were obtained from the linear fits of the inverse magnetic susceptibility vs temperature. The paramagnetic Weiss temperature θ_p and the effective magnetic moment of $Ce_7Li_8Ge_{10}$ and $Pr_7Li_8Ge_{10}$ are 3.3 K and 2.65 μ_B and 7.6 K and 3.68 μ_B, respectively (Figure 5). These effective magnetic moments are consistent with the magnetic behavior expected for free-ion RE^{3+} according to Hund's rules.[26] For $Pr_7Li_8Ge_{10}$, the onset of what appears to be antiferromagnetic ordering is seen at about 7 K.[27] The small positive θ_p value is not consistent with this conclusion, of course, but can be interpreted by considering that very weak ferromagnetic interactions could exist between the Pr^{3+} ions on different magnetic sublattices. These weak correlations are suppressed by

dx.doi.org/10.1021/ic300566x | *Inorg. Chem.* 2012, 51, 6821−6829

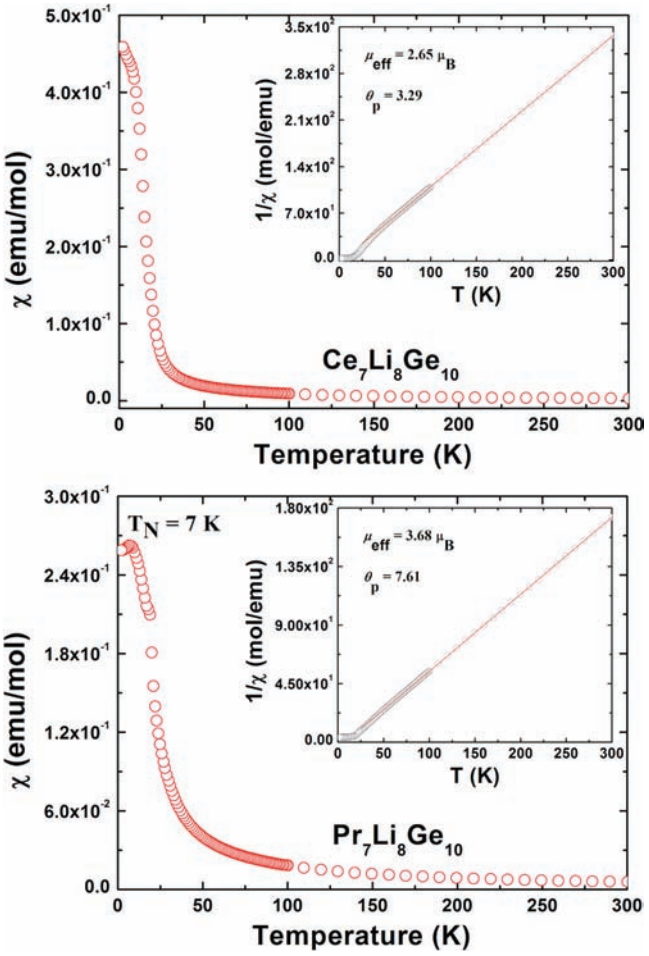

Figure 5. (Main Panels) DC magnetic susceptibility (χ) vs temperature of the $RE_7Li_8Ge_{10}$ (RE = Ce and Pr) compounds. Data were measured from 2 to 300 K under 5000 Oe. (Insets) Temperature dependence of the inverse magnetic susceptibility. Solid state red line is a fit of the data to the Curie–Weiss law.

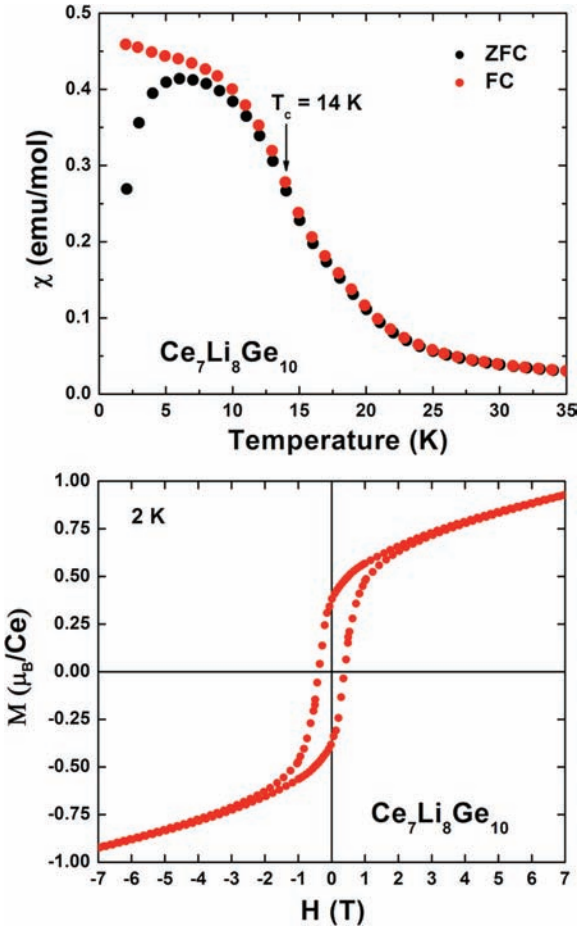

Figure 6. Field-cooled (red) and zero-field-cooled (black) magnetic susceptibilities (χ) vs temperature of $Ce_7Li_8Ge_{10}$ measured from 2 to 35 K (left). Magnetization vs applied field for $Ce_7Li_8Ge_{10}$ (right). Data was gathered at 2 K and normalized to the Bohr magneton (μ_B) unit.

the stronger antiferromagnetic interactions. A similar case was also found in $Pr_2Li_2Ge_3$. $Pr_2Li_2Ge_3$ and $Pr_3Li_4Ge_4$ also order antiferromagnetically.[7]

As shown in Figure 5, no apparent magnetic order can be detected down to the measured lowest temperature (2 K) for $Ce_7Li_8Ge_{10}$. The sharp increase of its magnetic susceptibility below 30 K, together with its positive θ_p, is a suggestion that it will likely transit into the ferromagnetic state at lower temperature. In order to verify this argument, the zero-field-cooled and field-cooled magnetic susceptibilities between 2 and 35 K together with the magnetization vs applied field were measured (Figure 6). An apparent divergence between ZFC and FC curves can be observed, and it is indicative of spin-glass behavior (most likely due to the presence of competing ferromagnetic and antiferromagnetic interactions). The corresponding ordering temperature, T_C = 14 K, was determined from the midpoint in the jump in $d\chi/dT$. The likely ferromagnetic transition at lower temperature is also verified by the hysteresis loop shown in Figure 6. From this loop, it can be observed that the magnetization of the $Ce_7Li_8Ge_{10}$ sample does not reach a plateau at 7 T, although the curvature suggests a strong tendency to saturate at lower temperature and/or higher fields. The maximum saturation moment is 0.93 μ_B per formula unit, much lower than the expected gJ value of 2.14 μ_B for a fully saturated Ce^{3+} moment.[26] However, the fact that there is a hysteresis also suggests that the dominant interactions are ferromagnetic like, but the nonsaturating behavior also supports the presence of the antiferromagnetic correlations.

This behavior is analogous to the magnetic responses of $Ce_2Li_2Ge_3$ and $Ce_3Li_4Ge_4$, which also order ferromagnetically at low temperatures. Although the ordering temperatures are in the same range, there are marked differences between the $Ce_7Li_8Ge_{10}$ and the $Ce_3Li_4Ge_4$ compounds most specifically; we are reporting only one magnetic transition for the former, while $Ce_3Li_4Ge_4$ was shown to undergo two magnetic ordering steps, accounted for by the presence of two inequivalent rare-earth metal atoms. For $Ce_7Li_8Ge_{10}$, where four inequivalent rare-earth metal atoms are present, the absence of more transitions could be explained assuming strongly correlated magnetic sublattices, resulting in complex (simultaneous) magnetic transitions. One could argue that a multitude of magnetic interactions likely exist in the material at low temperature, but they are not discernible by bulk magnetometry. Neutron diffraction—single crystal or powder—will be needed for complete characterization of the magnetic properties.

■ CONCLUSIONS

The crystal structures of the $RE_7Li_8Ge_{10}$ and $RE_{11}Li_{12}Ge_{16}$ (RE = La–Nd, Sm) compounds are closely related and contain $REGe_2$ fragments with the AlB_2 structure and $RELi_2Ge$

dx.doi.org/10.1021/ic300566x | Inorg. Chem. 2012, 51, 6821–6829

fragments with the $MgAl_2Cu$ structure and members of the $[REGe_2]_n[RELi_2Ge]_m$ homologous series. TB-LMTO-ASA calculations indicate that with 69 valence electrons per formula for the $RE_7Li_8Ge_{10}$ and with 109 valence electrons per formula for the $RE_{11}Li_{12}Ge_{16}$, both types of compounds are formally electron deficient, but adapt to the lower valence electron count and do not show signs of electronic instability. As a consequence, the mixing of Li and Ge in $RE_{11}Li_{12}Ge_{16}$ (rather $RE_{11}Li_{12-x}Ge_{16+x}$ ($x \approx 0.2$)) is hard to rationalize from the available information. Currently, we are pursuing more computational and experimental work geared toward $La_{11}Li_{12}Ge_{16}$, which is yet to be synthesized and characterized but could provide valuable information, particularly with regard to the electronic structure calculations. We are also interested in the extension of this chemistry to the *RE*−Li−Sn systems, where preliminary data indicate an unexpected wealth of new structures and bonding patterns.

■ ASSOCIATED CONTENT

Ⓢ Supporting Information

Combined X-ray crystallographic file in CIF format; figure showing a schematic representation of how the $RE_7Li_8Ge_{10}$ structure can be seen as 2:1 intergrowth of $RE_2Li_2Ge_3$ and $RE_3Li_4Ge_4$ fragments; tables with atomic coordinates, equivalent isotropic displacement parameters, and important distances for $RE_7Li_8Ge_{10}$ (*RE* = La, Pr, Nd, Sm) and $RE_{11}Li_{12}Ge_{16}$ (*RE* = Pr, Nd). This material is available free of charge via the Internet at http://pubs.acs.org.

■ AUTHOR INFORMATION

Corresponding Author

*Phone: (302) 831-8720. Fax: (302) 831-6335. E-mail: bobev@udel.edu.

Notes

The authors declare no competing financial interest.

■ ACKNOWLEDGMENTS

S.B. acknowledges financial support from the National Science Foundation through a grant DMR-0743916 (CAREER). Work at CBNU was supported by a research grant from the Chungbuk National University in 2011. The authors thank Dr. S. Saha, Prof. J. P. Paglione, and Prof. R. Greene (UMD) for the low-temperature measurement of $La_7Li_8Ge_{10}$.

■ REFERENCES

(1) Grin, Y. N. The Intergrowth Concept as a Useful Tool to Interpret and Understand Complicated Intermetallic Structures. In *Modern Perspectives in Inorganic Crystal Chemistry*; Parthé, E., Ed.; Kluwer Academic Publishers: Norwell, MA, 1992.

(2) In *Pearson's Handbook of Crystallographic Data for Intermetallic Phases*, 2nd ed.; Villars, P.; Calvert, L. D., Eds., American Society for Metals: Materials Park, OH, 1991.

(3) Chen, Y.; Liu, Q. L.; Liang, J. K.; Chen, X. L.; Shen, B. G.; Huang, F. *Appl. Phys. Lett.* **1999**, *74*, 856−858.

(4) Sologub, O. L.; Salamakha, L. P.; Noël, H.; Roisnel, T.; Gonçalves, A. P. *J. Solid State Chem.* **2007**, *180*, 2740−2746.

(5) (a) Latturner, S. E.; Kanatzidis, M. G. *Chem. Commun.* **2003**, 2340−2341. (b) Latturner, S. E.; Bilc, D.; Mahanti, S. D.; Kanatzidis, M. G. *Chem. Mater.* **2002**, *14*, 1695−1705. (c) Latturner, S. E.; Kanatzidis, M. G. *Inorg. Chem.* **2008**, *47*, 2089−2097.

(6) You, T.-S.; Tobash, P. H.; Bobev, S. *Inorg. Chem.* **2010**, *49*, 1773−1783.

(7) Guo, S.-P.; You, T.-S.; Bobev, S. *Inorg. Chem.* **2012**, *51*, 3119−3129.

(8) Andersen, O. A.; Jepsen, O.; Glötzel, D. In *Highlights of Condensed Matter Theory*; Bassani, F., Fumi, F., Tosi, M., Eds.; North-Holland: New York, 1985.

(9) Bobev, S.; You, T.-S.; Suen, N.-T.; Saha, S.; Greene, R.; Paglione, J. *Inorg. Chem.* **2012**, *51*, 620−629.

(10) You, T.-S.; Bobev, S. *J. Solid State Chem.* **2010**, *183*, 2895−2902.

(11) Nesper, R. *Prog. Solid State Chem.* **1991**, *1*, 1−45.

(12) *SMART NT*, version 5.63; Bruker Analytical X-ray Systems, Inc.: Madison, WI, 2003.

(13) *SAINT NT*, version 6.45; Bruker Analytical X-ray Systems, Inc.: Madison, WI, 2003.

(14) *SADABS NT*, version 2.10; Bruker Analytical X-ray Systems, Inc.: Madison, WI, 2001.

(15) *SHELXTL*, version 6.12; Bruker Analytical X-ray Systems, Inc.: Madison, WI, 2001.

(16) Gelato, L. M.; Parthé, E. *J. Appl. Crystallogr.* **1987**, *20*, 139−146.

(17) Jepsen, O.; Burkhardt, A.; Andersen, O. K. *The TB-LMTO-ASA Program*, version 4.7; Max-Planck-Institut für Festkörperforschung: Stuttgart, Germany, 1999.

(18) Jepsen, O.; Anderson, O. K. *Z. Phys. B* **1995**, *97*, 35−47.

(19) Anderson, O. K.; Jepsen, O. *Phys. Rev. Lett.* **1984**, *53*, 2571−2574.

(20) Lambrecht, W. R. L.; Andersen, O. K. *Phys. Rev. B* **1986**, *34*, 2439−2449.

(21) Dronskowski, R.; Blöchl, P. *J. Phys. Chem.* **1993**, *97*, 8617−8624.

(22) Pauling, L. *The Nature of the Chemical Bond*; Cornell University Press: Ithaca, NY, 1960.

(23) Suen, N.-T.; Tobash, P. H.; Bobev, S. *J. Solid State Chem.* **2011**, *184*, 2941−2947.

(24) (a) Guloy, A. M. Polar Intermetallics and Zintl Phases along the Zintl Border. *In Inorganic Chemistry in Focus III*; Wiley-VCH Verlag GmbH & Co. KGaA: Weinheim, Germany, 2006. (b) In *Chemistry, Structure and Bonding of Zintl Phases and Ions*; Kauzlarich, S. M., Ed.; VCH: Weinheim, Germany, 1996 and references therein.

(25) (a) Mudring, A.-V.; Corbett, J. D. *J. Am. Chem. Soc.* **2004**, *126*, 5277−5281. (b) Miller, G. J.; Lee, C.-S.; Choe, W. In *Inorganic Chemistry Highlights*; Meyer, G., Naumann, D., Wesemann, L., Eds.; Wiley-VCH: Berlin, 2002.

(26) (a) Smart, J. S. *Effective Field Theories of Magnetism*; Saunders: Philadelphia, PA, 1966. (b) Kittel, C. *Introduction to Solid State Physics*, 7th ed.; John Wiley and Sons: Hoboken, NJ, 1996.

(27) On the basis of the data, it is not possible to unambiguously determine if the transition at ca. 7 K is antiferromagnetic or not. While it may be so, most likely it is an additional magnetic transition that follows what seems to be 2 ferromagnetic-like transitions at higher temperatures.